THE RETRIEVAL OF CHLOROPHYLL-A CONCENTRATIONS IN INLAND WATER USING CONVOLUTION NEURAL NETWORK ON SATELLITE IMAGERY

Manh Van Nguyen[1,2], Chao-Hung Lin[2], Ariel C. Blanco[3]

[1]Institute of Geography, Vietnam Academy of Science and Technology, Hanoi 100000, Vietnam
Email: manh.ig239@gmail.com
[2]Department of Geomatics, National Cheng Kung University, Tainan 70101, Taiwan
Emails: p68087019@mail.ncku.edu.tw, linhung@mail.ncku.edu.tw
[3]Department of Geodetic Engineering, University of the Philippines, Diliman 1104, Philippines
Email: acblanco@upd.edu.ph

KEYWORD: Chlorophyll-a, Inland waters, Convolutional Neural Network, Sentinel-3 OLCI imagery.

ABSTRACT: The retrieval of chlorophyll-a (Chl-a) concentration, which is a crucial indicator in monitoring water quality across inland waters, remains a challenging task by using satellite data. Former studies based on semi-empirical and analytical approaches have achieved great progress. However, the Chl-a retrieval models from these approaches suffer from a wide range of uncertainties that originate from inter-seasonal variations of optical water properties and insufficient quantity of in situ samples. Most inland lakes in tropical regions experience different trophic states across wet and dry seasons. The optically water properties are complex and varied due to different trophic states over different seasons that pose difficulty to remote sensing-based models in accurately estimating Chl-a concentrations. To overcome this problem, a season-insensitive model based on a multi-task convolution neural network with a multi-output structure is proposed. In addition, a layer-sharing network structure with data augmentation is adopted to alleviate the problem of insufficient quantity of in situ Chl-a samples in model calibration and validation. To evaluate the proposed method, a largest lake in the Philippines, Laguna Lake, is selected as the study area. The lake is characterized by oligotrophic and mesotrophic conditions in wet season, whereas the states change to mesotrophic and eutrophic conditions in dry season. Several Sentinel-3 OLCI level-2 images matched with 409 in situ Chl-a measurements in range from 1.24 to 22.30 mg m^{-3} are collected. Over 5-fold cross validation, the average coefficient of determination (R^2) and root mean square error (RMSE) of the proposed model are 0.74 and 2.06 mg m^{-3}, respectively. In comparison, the estimation accuracy of our model is improved than that of related semi-empirical models. The slopes (m) of regressed lines generated from estimated and in situ Chl-a samples also demonstrate the ability of our proposed model to properly capture seasonal patterns of Chl-a in Laguna Lake.

1. INTRODUCTION

Eutrophication or nutrient over-enrichment has become one of the major concerns for inland waters, because it endangers sustainable socio-economic development and threatens human health (Ho et al. 2019; Wang et al. 2018). Previous studies determined that eutrophication, which is a qualitative assessment to measure the trophic states of water bodies, is positively correlated with chlorophyll-a (Chl-a) concentration (Liu et al. 2020; Zheng and Digiacomo 2017). Chl-a is an essential indicator linked with the changes of the biophysical states of inland waters (Moses et al. 2009; Neil et al. 2019). Thus, regular quantifying and monitoring the spatio-temporal distribution of Chl-a concentrations are vital in the evaluation of inland water quality (Gurlin et al. 2011). Since the successful ocean color mission of the Coastal Zone Color Scanner sensor mounted on Nimbus-7 satellite in 1978, satellite-based remote sensing approaches have been utilized to measure water quality for clear oceanic waters and inland turbid waters (Neil et al. 2019). Remote sensing is referred to as a labor-insensitive and cost-effective technology, which offers the advantage of providing spatially and temporally information of water surface bodies on a large scale, compared with traditional sampling methods (Kravitz et al. 2020).

Chl-a is an optically active constituent in water with peak absorption in blue and red spectrum regions; therefore, its concentration is measurable with the aid of optical satellite images (Meler et al. 2017). Based on the spectral characteristics, numerous algorithms relying on blue-to-green band ratios of remote sensing reflectance $R_{rs}(\lambda)$ were proposed. The empirical relationships between $R_{rs}(\lambda)$ reflectance and in situ Chl-a measurements are established by using statistical methods (Randolph et al. 2008; Zheng and Digiacomo 2017). These methods can obtain acceptable results of Chl-a concentration retrieval for clear oceanic waters, which are dominated by phytoplankton cells (Morel and Prieur 1977). However, for inland turbid waters (e.g., lakes, reservoirs, and rivers), these algorithms experienced unstable performances (Vilas et al. 2011). The optically water properties of inland waters are complicated, because the high and varied absorption spectrums of colored dissolved organic matter (CDOM) and detritus particles do not covary with the Chl-a concentration,

that generally limit the effectiveness of the aforementioned methods (Palmer et al. 2015; Zheng and Digiacomo 2017). There is another method to retrieve Chl-a concentration of inland turbid waters is based on red-to-near infrared band ratios. These band ratios may consist of two, three, or four spectral bands, in which the red band at 665 nm is compulsory and the other bands are selected from near-infrared spectrum, nearby 700 nm and 754 nm (Liu et al. 2020).
Considering that the relationship between Chl-a concentrations of inland waters and their spectral signatures in optical satellite images is non-linear and complicated, an artificial neural network (ANN) that has been proven effective in nonlinear modeling was applied to retrieve Chl-a concentrations (Blix et al. 2019; Hafeez et al. 2019; Pahlevan et al. 2020; Su et al. 2021). In addition to the feedforward ANN, convolutional neural network (CNN) has become a promising structure for processing multidimensional satellite images in Chl-a retrievals, the CNN is capable of extracting spatial and spectral features of satellite images using convolution operators with kernel filters (Cao et al. 2020; Kim et al. 2014; Pyo et al. 2019; Vilas et al. 2011).

Although the empirical band ratios, ANNs and CNN-based approach provide promising results, the uncertainties in different biophysical properties of inland waters in different seasons have not been fully studied. Uncertainties caused by different seasons may decrease the robustness and accuracy of Chl-a concentration measurement. In this study, a season-insensitive model based on a multi-task convolutional neural network is proposed. In addition, the problem of limited in situ samples is alleviated by using transfer learning with layer-sharing network structure and data augmentation. The remainder of the paper is organized as follows. Section 2 describes the study area, problem statement, data acquisition, and preprocessing. Section 3 presents the methodology. Sections 4 and 5 provide the experimental results and conclusions, respectively.

2. STUDY AREA AND MATERIALS

2.1 Study area

The study selected Laguna Lake as the study area. It is located southeast of Metro Manila, Philippines, as shown in Figure 1. The Laguna Lake is the largest lake in the Philippines, covering a surface area of 900 km^2 with an average depth of 2.5 m (Hallare et al. 2005). The lake is formed by three distinct bays, that is, East Bay, West Bay, and Central Bay. Although Laguna Lake serves as a vital water supply, the water resource has been greatly affected by population growth and rapid industrialization since the last decade (Bongco et al. 2003).

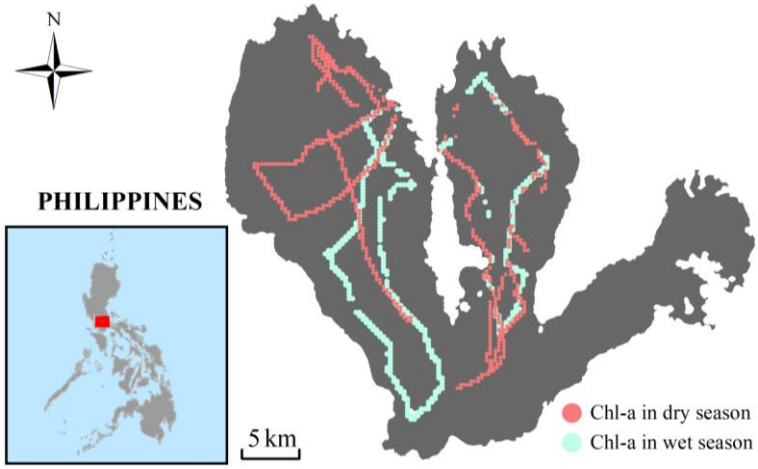

Figure 1. Study area. Laguna Lake, marked by white border, is selected as the study area. The locations of in situ Chl-a samples in dry and wet seasons are illustrated by yellow and red portions, respectively.

Two distinct seasons, that is, dry and wet seasons, can be climatically recognized in Laguna Lake. The dry season begins in December and ends in May, and the wet season occurs from June to November (Jalbuena et al. 2019). The lake hydrological system is complex and varies according to season. When the lake gains a large amount of precipitation from several tropical cyclones in wet season, the mean water level of the lake is estimated to increase by one meter higher than the mean sea level in Manila Bay. The water flows from the lake toward Manila Bay through the Pasig river, which is known as the only outlet of the lake. By contrast, at certain periods of high tide in Manila Bay and low water level in the lake, which frequently occur during the dry season, the Pasig river reverses its flow direction, bringing saline water from

Manila Bay and polluted water from industrial and domestic effluents to the lake (Santos-Borja 1994). Therefore, the lake exhibits a marked inter-lake variation in trophic states. The lake is classified as oligotrophic and mesotrophic states in the wet season, whereas the states change to mesotrophic and eutrophic states in dry season. This change may influence the optical properties of water and increase the difficulty of water quality estimation by using remote sensing approaches.

2.2 Data Collection and Preprocessing

Five and two field campaigns in dry and wet seasons, respectively, were conducted from November 2018 to May 2019. Owing to high cloud coverages, the number of field campaigns in wet seasons is less than that in dry season. In each campaign, the boat was equipped with an optical-based data logger, which can record the concentration of Chl-a per second. In situ Chl-a samples were collected within ± 2 hours of the local overpass time of the Sentinel-3 satellite, thereby reducing the possibility of inconsistency between the collected in situ Chl-a samples and optical satellite images. After the removal of sample outliers, the collected samples are downsampled to match with the spatial resolution of satellite images, that is, 300 m. After data preprocessing, a total of 409 Chl-a samples were obtained, consisting of 275 samples in dry season and 134 samples in wet season. Table 1 shows the information of the processed Chl-a samples and their corresponding satellite images.

Table 1. Statistics of the processed Chl-a samples. The minimal, maximal, and standard deviation of the processed Chl-a concentrations are denoted by Min., Max., and St. Dev., respectively.

Season	Field campaigns	N	Chlorophyll-a (mg m^{-3})			
			Min.	Max.	Mean	St. Dev.
Dry	01-11-2019	23	5.85	18.50	12.47	3.67
	03-29-2019	69	4.64	8.81	6.44	0.85
	04-06-2019	37	5.93	10.85	7.74	1.09
	04-26-2019	29	6.48	8.87	7.40	0.78
	04-30-2019	117	6.51	22.30	12.36	4.10
Wet	11-06-2018	55	2.22	13.68	6.91	3.02
	11-14-2018	79	1.24	13.07	6.63	3.08

Seven Sentinel-3 OLCI Level-2 Water (L2W) images, which are synchronous with the dates of field campaigns, were downloaded from the EUMESAT Copernicus Online Data Access. The Sentinel-3 L2W images were atmospherically corrected (AC) by the alternative atmospheric correction algorithm (AAC), providing normalized water-leaving reflectance, these reflectance then divided by π to obtain remote sensing reflectance, denoted as $R_{rs}(\lambda)$, of 16 spectral bands. In the image preprocessing, the boundary shapefile of the study area was used to extract water pixels in the lake. Then, a series of cloud-contaminated pixels, ambiguous cloud pixels, negative pixels, and AC-failed pixels were determined and excluded using corresponding masks in the L2W images.

3. METHODOLOGY

3.1 Multi-task Convolutional neural network (MCNN)

A CNN model generally consists of three main functional layers, that is, convolution layer, pooling layer, and fully connected layer. The convolution layers based on weight-sharing architecture and translation-invariant characteristics are known as parameter-efficient and shift-invariant layers. In pooling layers, the sizes of feature maps come from convolutional layers and the amount of parameters are reduced, which can reduce the possiblity of overfitting. The fully connected layers taking the feature maps as inputs are used to predict Chl-a concentrations.

A season-insensitive model based on multi-task CNN with a multi-output structure (MCNN) is proposed. The MCNN model simultaneously handles two tasks in the network, that is, season classification and Chl-a concentration regression, with a single input image. The Chl-a concentration regression is the major task, whereas the season classification is an auxiliary task. The main idea is to employ the classification probability results in the auxiliary task to assist the determination of Chl-a concentration in the regression performance. Figure 2 illustrates the network structure of the proposed model. A spectral convolutional layer containing three spectral kernels ($1 \times 1 \times 3$) is performed to extract spectral patterns of the input images. Unlike traditional CNNs that perform convolution operators on the spatial domain, the CNN layer in our model addresses the spectral features in spectral domain. The spectral kernel ($1 \times 1 \times 3$) is used in the convolution layer, which makes the model possess the property of spectral shift invariance. Owing to the spectral shift

invariance, the spectral feature patterns for Chl-a concentration measurements can be efficiently extracted under the convolution operators.

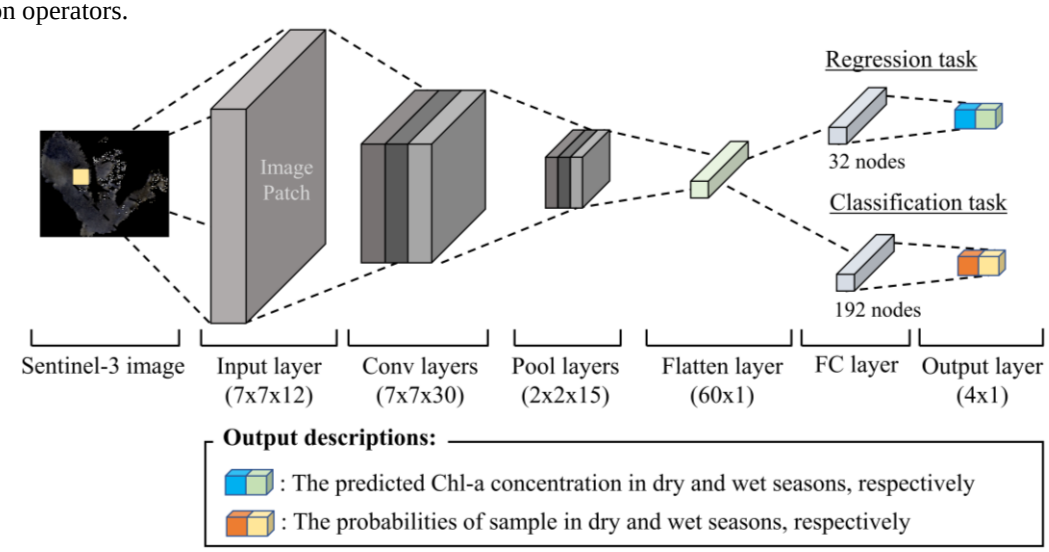

Figure 2. The architecture of our CNN-based Chl-a retrieval model.

The layers of batch normalization and pooling are added after the spectral convolutional layer. Maximal pooling with the grid size $(2 \times 3 \times 3)$ is implemented to retain spectral features. The 2D spectral features are then flattened to a 1D tensor. The flattened layer is connected to two different fully connected branches for the tasks of season classification and Chl-a concentration regression. The first branch consists of a fully-connected layers containing 32 neurons for season classification. The second branch has one fully-connected layer containing 192 neurons for Chl-a concentration prediction. The outputs of two branches contain four neurons representing two predicted Chl-a concentrations and two classify probabilities of sample in wet and dry seasons. Given the two-task neural structure, the loss function is defined as a weighted combination of the sub-losses from the two tasks. The loss in the Chl-a concentration regression task is defined by using RMSE, whereas the loss in the season classification task is measured by using binary cross-entropy, which will be described in Section 3.5.

3.2 Input and output tensors

The input to MCNN model is a 3D image patch that measures 12 (spectral bands) × 7 (width) × 7(height) to utilize spectral and spatial information in Chl-a concentration modeling. An image patch is centered at the location of a sampling point, and the estimated Chl-a concentration links to the center pixel of the image patch. Twelve spectral bands in the Sentinel-3 OLCI bands with wavelength ranging from 400 nm to 753 nm are utilized as model inputs. All pixel values $R_{rs}(\lambda)$ in image pathes are rescaled to [0.0, 1.0] by means of min-max normalization.

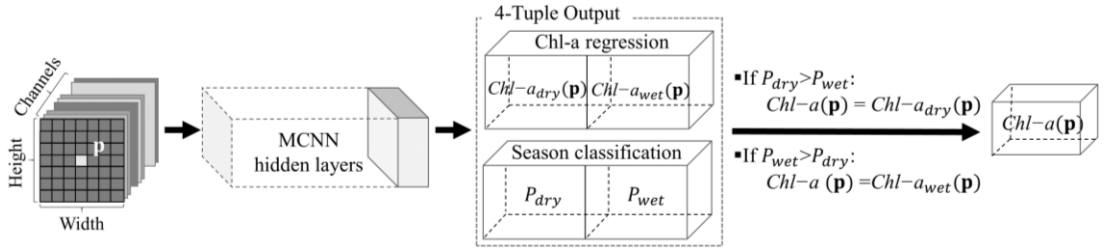

Figure 3. The output layer have four neurons. Two neurons are the predicted Chl-a in dry and wet seasons for the regression task, and other two neurons are the probabilities of samples in dry and wet seasons for the classification task.

The output layer contains four neurons as shown in Figure 3. Two neurons represent the Chl-a concentration of center pixel **p** of the image patch in the dry and wet seasons, denoted as $Chla_{dry}(\mathbf{p})$ and $Chla_{wet}(\mathbf{p})$, and another two neurons present the season probabilities of the image patch, denoted as P_{dry} and P_{wet}. The final output is the predicted Chl-a concentration with the highest season probability, which is formulated as

$$Chl\text{-}a\ (\mathbf{p}) = \begin{cases} Chla_{\ dry}(\mathbf{p}), & if\ P_{dry} > P_{wet} \\ Chla_{wet}(\mathbf{p}), & if\ P_{wet} > P_{dry} \end{cases}. \quad (1)$$

The data used in model training are image patches with 2-tuple ground truths containing the entries of Chl-a concentration and data acquisition season. In preprocessing, the 2-tuple ground truth is extended to 4-tuple ground truth, that is, $(Chla_{dry}(\mathbf{p}), Chla_{wet}(\mathbf{p}), P_{dry}, P_{wet})$, to fit with the tensor shape of model outputs. For the entries of the season classification subtuple, the probability of the data acquisition season is set to 1.0, and the probability of another season is set to 0.0. For the entries of the Chl-a concentration subtuple, one entry is set to the ground-truth value and another entry is a synthetic value. Given that Chl-a concentrations are normalized to the range [0.0, 1.0], the synthetic values of Chl-a concentration are set to −0.2, which is outside of the normalized range. For instance, the 2-tuple ground truth (0.8, dry season) is extended to the 4-tuple (0.8, −0.2, 1.0, 0.0), representing that the Chl-a concentrations are 0.8 and −0.2 for dry and wet seasons, respectively, and the probabilities of dry and wet seasons are 1.0 and 0.0, respectively.

3.3 Transfer learning

To alleviate the problem of insufficient quantity of in situ samples in model training, two-stage transfer learning containing pre-training and fine-tuning stages, as shown in Figure 4, is adopted. The MCNN model is initially trained using Chl-a concentrations generated by an existing Chl-a estimator, and the pre-trained model is then fine-tuned using the in situ Chl-a concentrations from field surveys. With the aid of existing Chl-a estimators, a huge set of training samples can be generated to fulfill the requirement of model training. The pre-trained model containing initial weights and biases of the network is further fine-tuned using a small set of in situ Chl-a concentrations. With the two-stage transfer learning, the problem of insufficient quantity of in situ samples can be efficiently alleviated.

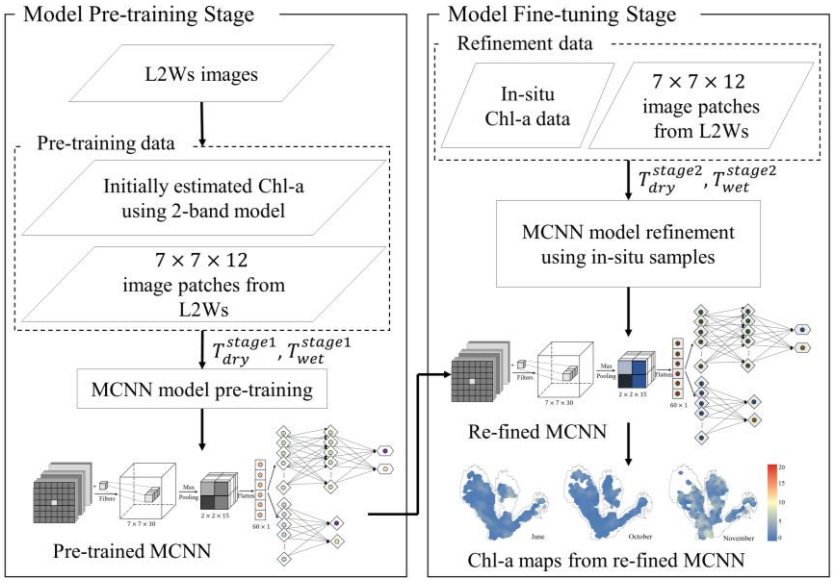

Figure 4. The two-stage transfer learning consists of model pre-training stage (left) and model fine-tuning stage (right)

The inputs to the algorithm in the first stage are the remote sensing reflectances $R_{rs}(\lambda)$ at all sampling locations extracted from the Sentinel-3 L2W images and the pre-estimated Chl-a concentrations generated by the two-band Chl-a estimation model (Gitelson et al. 2008), that is, $R_{rs}(754)/R_{rs}(665)$. Note that a simple model is adopted in the first stage, because the pre-estimated Chl-a concentrations used to pre-train the MCNN model and model will be further refined in the second stage. The generated Chl-a concentrations with the corresponding Sentinel-3 L2W images are utilized to form the pretraining datasets $T_{dry}^{stage1} = \{(\mathbf{P}_i, ns\_Chl_{dry,i})\}_{i=1}^{n_1}$ and $T_{wet}^{stage1} = \{(\mathbf{P}_j, ns\_Chl_{wet,j})\}_{j=1}^{m_1}$ for dry and wet seasons, respectively, where $\mathbf{P} = \{Rrs_1, \cdots, Rrs_{588}\}$ containing 588 values (7 × 7 [pixels] ×12 [bands]) denotes an image patch of an L2W image and ns_Chl represents the corresponding Chl-a concentration at the center pixel of the patch. n_1 and m_1 denote the numbers of patches in dry and wet seasons, respectively. Given the classification task in MCNN model, the numbers of pretraining samples for dry and wet seasons, that is, n_1 and m_1, shall be similar to avoid the problem of data imbalance. In addition to the pretraining datasets, a set of in situ samples $T_{dry}^{stage2} = \{(\mathbf{P}_k, meas\_Chl_{dry,k})\}_{k=1}^{n_2}$ and

$T_{wet}^{stage2} = \{(\mathbf{P}_p, meas\_Chl_{wet,p})\}_{p=1}^{m_2}$ in dry and wet seasons is used for model refinement in the second stage, where n_2 and m_2 represent number of in situ samples in dry and wet seasons, respectively. $meas\_Chl$ denotes the in situ Chl-a value. The datasets used in the mode refinement are augmented by using data augmentation, which will be described in Section 3.4.

3.4 Data augmentation and balancing

The training of ANN models relies on the collection of sufficient and various training samples. Training an ANN model using a small set of training samples may cause overfitting. However, the collection of a large volume of in situ data is labor-intensive and cost-sensitive. To alleviate this problem, data augmentation, which is a technique to increase the size and diversity of training dataset by adding modified copies of already existing data on the basis of transformation operators, is performed. The various transformations of rotation and flipping are applied to image patches $\mathbf{P}_k$ in T_{dry}^{stage2} and $\mathbf{P}_p$ in T_{wet}^{stage2} because the spatial and spectral features of image patches are isotropic and rotation invarient, as shown in Figure 5. The Chl-a concentration of an image patch links to the center pixel; thus, the Chl-a concentrations are unchanged after these transformations. The setting for 11 augmentation transformations in this study are described in Table 2.

In addition, dataset imbalance, that is, the numbers of samples in majority classes are much larger than that in minority classes, will decrease the generalization of minority classes in blind testing. To avoid the problem of data imbalance, the numbers of collected pretraining samples in T_{dry}^{stage1} and T_{wet}^{stage1}, need to be similar, that is, $n_1 \cong m_1$.

Table 2. Setting for augmentation transformations in this study

Transformations	Settings
Rotation	rotate with an angle of 90^0, 180^0, and 270^0
Flipping	[left to right] or [top to bottom]
Rotation and flipping	rotate with an angle in [90^0, 180^0, 270^0] and then flip from [left to right] or [top to bottom]

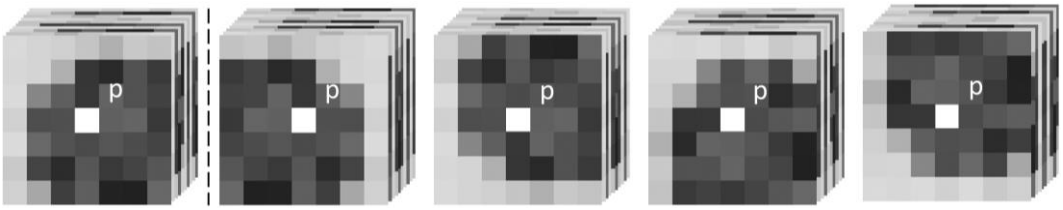

Figure 5. Data augmentation example. Left: original 7 × 7 image patch (left). Right (from left to right): data augmentation results using vertical flipping, horizontal flipping, rotation, and vertical flipping with rotation.

3.5 Cost function

The CNN-based model consists of the tasks of regression (major task) and classification (auxiliary task). Thus, the loss function contains two sub-loss terms for these two tasks. The regression term is measured by using RMSE as follows:

$$Loss_{reg} = \sqrt{\frac{1}{n_2+m_2}\sum_{k=1}^{n_2+m_2}(pred\_Chl_k - meas\_Chl_k)^2}, \quad (2)$$

where $pred_k$ represents the Chl-a concentration prediction result from the refined model. The term for classification is defined by using binary cross-entropy as follows:

$$Loss_{cls} = -\sum_{k=1}^{n_2+m_2}\begin{Bmatrix} pred\_Chl_k \times log(meas\_Chl_k) + \\ (1 - pred\_Chl_k)\log(1 - meas\_Chl_k) \end{Bmatrix}. \quad (3)$$

The total loss is defined as combining these two terms with weights, that is,

$$T\_Loss = \lambda\, Loss_{reg} + (1 - \lambda)\, Loss_{cls}, \quad (4)$$

where weight λ is used to balance the combinations of regression and classification terms. In the experiments, λ is set to 0.7 to enhance the contributions from the main task.

4. EXPERIMENTAL RESULTS AND DISCUSSION

In model training, Adam (Diederik and Ba 2017) is selected as the optimizer. The learning rate is set to 0.0007, and the number of epochs is set to 100. Considering the stability of model training, the Chl-a concentrations (ns_Chl and $meas\_Chl$) and remote sensing reflectances ($\mathbf{P} = \{Rrs_1, \cdots, Rrs_{588}\}$) in training and testing samples are normalized to the range [0.0, 1.0] in data preprocessing. The outputs are rescaled back to their original ranges in postprocessing. To prevent model overfitting, L_2 regularization (Hastie et al. 2009) is applied to the layers, and the penalty factor is set to 0.1.

The MCNN model is trained by using two-stage learning, that is, pretraining and refinement stages. The satellite images used in pre-training stage are acquired from November 2018 to May 2019, and the corresponding Chl-a concentrations are roughly estimated by using a two-band model (Gitelson et al. 2008), that is $Chl - a = -5.62 \times \frac{R_{rs}(754)}{R_{rs}(665)} + 20.06$. To avoid data imbalace, the equivalent numbers of pretraining samples in dry and wet seasons are generated. There are 12,777 and 11,221 dry- and wet-season patches, respectively. The fine-tuning stage involves 275 and 134 in situ measurements in dry and wet seasons from field surveys. Noted that a k-fold (k=5) cross-validation will be applied in the second stage, in which 80% of total in situ samples is considered for refining model, correspond to 220 dry- and 107 wet-season samples. During the cross-validation, there four folds (n=327) were selected to refine the pre-trained model, and the remaining fold (n=82) was used for validation. The patches of 327 in situ samples in the refinement folds were augmented by the 11 transformations as listed in Table 2. After augmentation, there were 3924 training patches containing 3597 augmented patches and 327 original patches. The remaining 20% of total in situ samples, correspond to 55 dry- and 27 wet-season samples, the patches of these samples are preserved as original, used for validating model.

To evaluate the performance of our proposed model MCNN, the R^2 and RMSE are used to measure the accuracy of the predicted Chl-a concentrations. In addition, linear regression is performed on the measured and predicted Chl-a concentrations. The slope, denoted as m, of the fitting line is used to measure the correlation of these two concentrations. In this section, Section 4.1 presents the performance and the comparisons of MCNN model with related semi-empirical models. Section 4.2 presents the generated seasonal Chl-a concentration maps.

4.1 Performance of the MCNN model and comparison to related semi-empirical models

Over 5-fold cross-validation, our model results the average R^2 and RMSE are of 0.74 and 2.06, respectively. To evaluate the performance of the MCNN model, the model was compared with related red-to-NIR methods, including the methods based on two-band ratio (denoted as $NIRR_1$) (Moses et al. 2009), two-band ratio (denoted as $NIRR_2$) (Gitelson et al. 2008), three-band ratio (denoted as $NIRR_3$) (Gitelson et al. 2008), and NDCI (denoted as $NIRR_4$) (Mishra and Mishra 2012). These methods are able to quantify Chl-a concentration in turbid productive waters. Table 6 lists the models of these related methods.

Figure 8 shows the comparison results. The red-to-NIR methods produced acceptable results with RMSE of 2.53 to 3.69 mg m^{-3}. Nevertheless, the determination of coefficient R^2 obtained from these models is relatively low due to the CDOM absorption at those regions of the spectrum. In inland water bodies, non-algal particles such as suspended sediments do not covary with Chl-a. Thus, the correlation between algorithm-derived Chl-a and in situ Chl-a is low and generally overestimated compared with field measurements. By contrast, our model showed better accuracy (average R^2: 0.74 and average RMSE: 2.06 mg m^{-3}) in dry and wet seasons.

Figure 9 shows a detailed comparison the slope of best fit line (m) between in situ and model-derived Chl-a. The comparison shows that the proposed model consistently achieves better estimation of Chl-a concentration than band-ratio-based methods in dry and wet season.

Table 6. Summary of related Chl-a retrieval models and their applicable Chl-a range (mg m^{-3}).

Model	Notation	Equation	Chl-a range (mg m^{-3})
Two-band model (Moses et al. 2009)	$NIRR_1$	$\frac{R_{rs}(709)}{R_{rs}(665)}$	[4, 236]
Two-band model (Gitelson et al. 2008)	$NIRR_2$	$\frac{R_{rs}(754)}{R_{rs}(665)}$	[4, 236]
Three-band model (Gitelson et al. 2008)	$NIRR_3$	$\left[\frac{1}{R_{rs}(665)} - \frac{1}{R_{rs}(709)}\right] \times R_{rs}(754)$	[4, 236]
NDCI (Mishra and Mishra 2012)	$NIRR_4$	$\frac{[R_{rs}(709) - R_{rs}(665)]}{[R_{rs}(709) + R_{rs}(665)]}$	[0.9, 28.1]

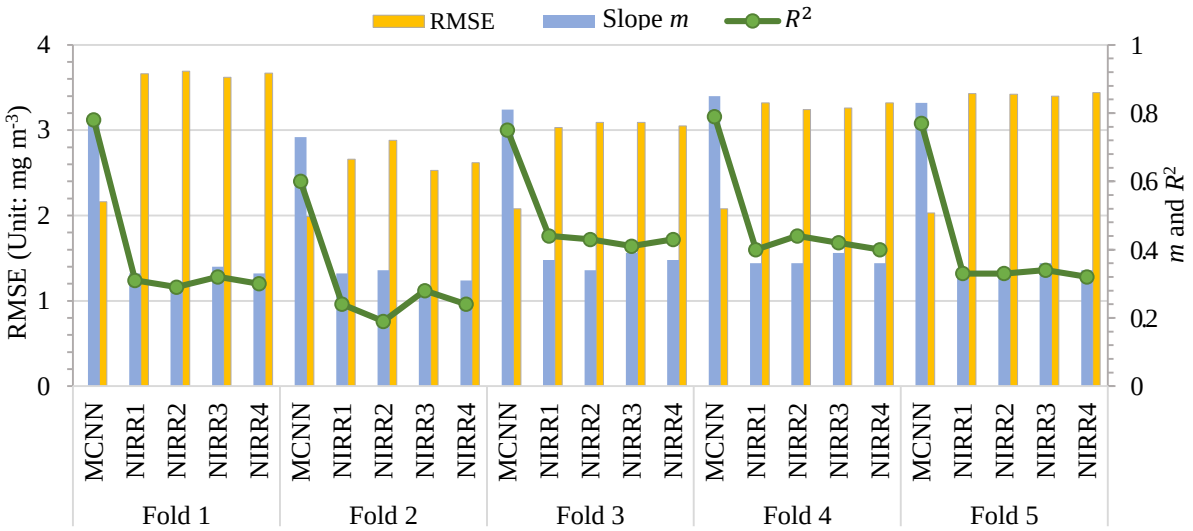

Figure 8. Comparison of the optimized MCNN model with the related Chl-a retrieval models. RMSE (left), slope *m* and R^2 (right) are used as measurements.

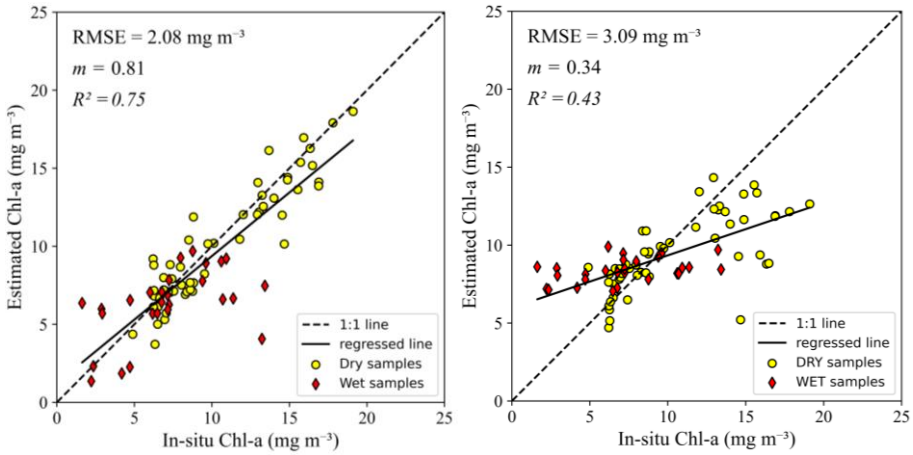

Figure 9. Comparison of MCNN (left) and two-band model $NIRR_2$ (right) in fold 3. The scatterplots reveal the correlation between in situ and model-derived Chl-a concentrations.

4.2 Spatial-seasonal variation of Chl-a concentration

The trained model was applied to several Sentinel-3 OLCI imagery. Figure 10 shows the results of predicted Chl-a concentrations. Seasonality was well captured in the visualization, and the complex spatial variability of Chl-a concentrations was clearly displayed. Relatively low Chl-a concentrations are found in wet months, including June,

October, and November; and relatively high Chl-a concentrations appear in dry months, including January, March, and April. One of the possible reasons is the change of hydrological regime. Tropical storms generally approach the Philippines in wet seasons, which bring a large amount of precipitation and turn the lake into turbid conditions. The water level is also higher than that in Manila Bay, which reverses the flow directions from the lake to Manila Bay and brings nutrients out through the Pasig River. The pollution level is relatively low at that time. During dry season, the lake water level is lower than that in Manila Bay. Some nutrients and waste waters from Manila Bay and Pasig River flow into the lake, thereby worsening the lake's pollution level. The Chl-a concentration maps shown in Figure 10 fit well with the local conditions and seasonal cycle of Chl-a concentrations.

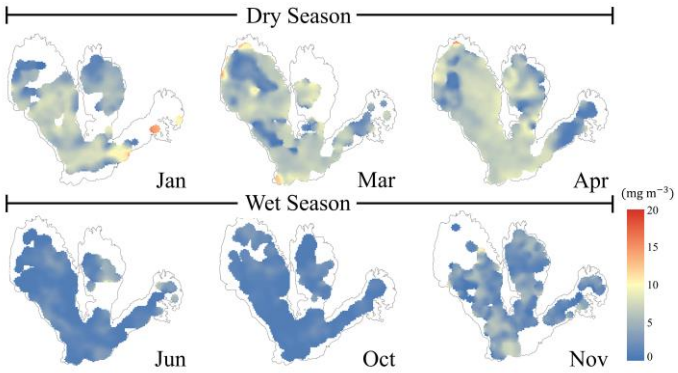

Figure 10. Spatial-temporal maps of Chl-a concentration produced by the MCNN using Sentinel-3 OLCI images acquired from 2018 to 2019. The low to high Chl-a concentrations are visualized by a blue-to-red color scheme.

5. CONCLUSIONS AND FUTURE WORKS

A season-insensitive Chl-a concentration retrieval model based on multi-task CNN is proposed to retrieve Chl-a concentrations in inland waters with complex hydrological regime using optical satellite images. The Laguna Lake, which is characterized by oligotrophic and mesotrophic states in the wet season and eutrophic and mesotrophic states in the dry season, is selected as the study area. According to the experimental results, the following conclusions are made. The integration of data augmentation, and two-stage training technique helps overcome the limitation of small in situ dataset. Such integration can prevent overfitting during MCNN model training and improve the model's generalization in Chl-a concentration estimation. In the estimation of Chl-a concentrations, the average RMSE and coefficient of determination R^2 are 2.06 and 0.74, respectively, which outperform that of related NIRR methods. Although the NIRRs are the well-documented models for Chl-a concentration estimation in inland turbid water bodies, the estimated Chl-a concentrations are sometimes not highly correlated with field measurements in dry and wet seasons. Hence, the relationships between the R_{rs} spectral patterns and Chl-a concentrations vary seasonally. However, with the aid of multi-task network structure, the estimations of Chl-a concentrations in dry and wet seasons are integrated into a network, which makes the MCNN model insensitive to optical images acquired in different seasons.

In future, the model could be further improved when a global scale and multi-temporal in situ samples is avaliable. We also attempt to faciliate the MCNN model to estimate other optically active water constitutuents in addition to Chl-a concentration.

REFERENCES

Blix, K., Li, J., Massicotte, P., & Matsuoka, A. (2019). Developing a New Machine-Learning Algorithm for Estimating Chlorophyll-a Concentration in Optically Complex Waters: A Case Study for High Northern Latitude Waters by Using Sentinel 3 OLCI. Remote Sensing, 11, 2076

Bongco, I.G., Santos-Borja, A.C., & Nauta, T.A. (2003). Application of habitat evaluation procedure for impact assessment studies in Laguna de Bay, Philippines. Hydrobiologia, 506, 811-817

Cao, Z., Ma, R., Duan, H., Pahlevan, N., Melack, J., Shen, M., & Xue, K. (2020). A machine learning approach to estimate chlorophyll-a from Landsat-8 measurements in inland lakes. Remote Sensing of Environment, 248, 111974

Diederik, & Ba, J. (2017). Adam: A Method for Stochastic Optimization. arXiv pre-print server

Freitas, F.H., & Dierssen, H.M. (2019). Evaluating the seasonal and decadal performance of red band difference algorithms for chlorophyll in an optically complex estuary with winter and summer blooms. Remote Sensing of Environment, 231, 12

Gitelson, A.A., Dall'Olmo, G., Moses, W., Rundquist, D.C., Barrow, T., Fisher, T.R., Gurlin, D., & Holz, J. (2008). A simple semi-analytical model for remote estimation of chlorophyll-a in turbid waters: Validation. Remote Sensing of Environment, 112, 3582-3593

Gurlin, D., Gitelson, A.A., & Moses, W.J. (2011). Remote estimation of chl-a concentration in turbid productive waters - Return to a simple two-band NIR-red model? Remote Sensing of Environment, 115, 3479-3490

Hafeez, S., Wong, M., Ho, H., Nazeer, M., Nichol, J., Abbas, S., Tang, D., Lee, K., & Pun, L. (2019). Comparison of Machine Learning Algorithms for Retrieval of Water Quality Indicators in Case-II Waters: A Case Study of Hong Kong. Remote Sensing, 11, 617

Hallare, A., Kosmehl, T., Schulze, T., Hollert, H., Kohler, H., & Triebskorn, R. (2005). Assessing contamination levels of Laguna Lake sediments (Philippines) using a contact assay with zebrafish (Danio rerio) embryos, 347, 254-271

Ho, J.C., Michalak, A.M., & Pahlevan, N. (2019). Widespread global increase in intense lake phytoplankton blooms since the 1980s. Nature, 574, 667-670

Jalbuena, R.L., Blanco, A.C., Manuel, A., Sta. Ana, R.R., & Santos, J.A. (2019). BIO OPTICAL MODELLING OF LAGUNA LAKE USING BOMBER TOOL AND WASI-DERIVED INVERTED PARAMETERS. ISPRS - International Archives of the Photogrammetry, Remote Sensing and Spatial Information Sciences, XLII-4/W16, 277-282

Kim, Y.H., Im, J., Ha, H.K., Choi, J.-K., & Ha, S. (2014). Machine learning approaches to coastal water quality monitoring using GOCI satellite data. GIScience & Remote Sensing, 51, 158-174

Kravitz, J., Matthews, M., Bernard, S., & Griffith, D. (2020). Application of Sentinel 3 OLCI for chl-a retrieval over small inland water targets: Successes and challenges. Remote Sensing of Environment, 237, 111562

Liu, G., Li, L., Song, K., Li, Y., Lyu, H., Wen, Z., Fang, C., Bi, S., Sun, X., Wang, Z., Cao, Z., Shang, Y., Yu, G., Zheng, Z., Huang, C., Xu, Y., & Shi, K. (2020). An OLCI-based algorithm for semi-empirically partitioning absorption coefficient and estimating chlorophyll a concentration in various turbid case-2 waters. Remote Sensing of Environment, 239, 111648

Meler, J., Ostrowska, M., Ficek, D., & Zdun, A. (2017). Light absorption by phytoplankton in the southern Baltic and Pomeranian lakes: mathematical expressions for remote sensing applications. Oceanologia, 59, 195-212

Mishra, S., & Mishra, D.R. (2012). Normalized difference chlorophyll index: A novel model for remote estimation of chlorophyll-a concentration in turbid productive waters. Remote Sensing of Environment, 117, 394-406

Morel, A., & Prieur, L. (1977). Analysis of variations in ocean color1. Limnology and Oceanography, 22, 709-722

Moses, W.J., Gitelson, A.A., Berdnikov, S., & Povazhnyy, V. (2009). Satellite Estimation of Chlorophyll-a Concentration Using the Red and NIR Bands of MERIS-The Azov Sea Case Study. Ieee Geoscience and Remote Sensing Letters, 6, 845-849

Neil, C., Spyrakos, E., Hunter, P.D., & Tyler, A.N. (2019). A global approach for chlorophyll-a retrieval across optically complex inland waters based on optical water types. Remote Sensing of Environment, 229, 159-178

Pahlevan, N., Smith, B., Schalles, J., Binding, C., Cao, Z., Ma, R., Alikas, K., Kangro, K., Gurlin, D., Hà, N., Matsushita, B., Moses, W., Greb, S., Lehmann, M.K., Ondrusek, M., Oppelt, N., & Stumpf, R. (2020). Seamless retrievals of chlorophyll-a from Sentinel-2 (MSI) and Sentinel-3 (OLCI) in inland and coastal waters: A machine-learning approach. Remote Sensing of Environment, 240, 111604

Palmer, S.C.J., Kutser, T., & Hunter, P.D. (2015). Remote sensing of inland waters: Challenges, progress and future directions. Remote Sensing of Environment, 157, 1-8

Pyo, J., Duan, H., Baek, S., Kim, M.S., Jeon, T., Kwon, Y.S., Lee, H., & Cho, K.H. (2019). A convolutional neural network regression for quantifying cyanobacteria using hyperspectral imagery. Remote Sensing of Environment, 233, 111350

Randolph, K., Wilson, J., Tedesco, L., Li, L., Pascual, D.L., & Soyeux, E. (2008). Hyperspectral remote sensing of cyanobacteria in turbid productive water using optically active pigments, chlorophyll a and phycocyanin. Remote Sensing of Environment, 112, 4009-4019

Santos-Borja, A.C. (1994). The Control of Saltwater Intrusion into Laguna de Bay: Socioeconomic and Ecological Significance. Lake and Reservoir Management, 10, 213-219

Su, H., Lu, X., Chen, Z., Zhang, H., Lu, W., & Wu, W. (2021). Estimating Coastal Chlorophyll-A Concentration from Time-Series OLCI Data Based on Machine Learning. Remote Sensing, 13, 576

Vilas, L.G., Spyrakos, E., & Palenzuela, J.M.T. (2011). Neural network estimation of chlorophyll a from MERIS full resolution data for the coastal waters of Galician rias (NW Spain). Remote Sensing of Environment, 115, 524-535

Wang, S., Li, J., Zhang, B., Spyrakos, E., Tyler, A.N., Shen, Q., Zhang, F., Kuster, T., Lehmann, M.K., Wu, Y., & Peng, D. (2018). Trophic state assessment of global inland waters using a MODIS-derived Forel-Ule index. Remote Sensing of Environment, 217, 444-460

Zheng, G., & Digiacomo, P.M. (2017). Remote sensing of chlorophyll-a in coastal waters based on the light absorption coefficient of phytoplankton. Remote Sensing of Environment, 201, 331-341